Materials Today Bio 31 (2025) 101633

Contents lists available at ScienceDirect

Materials Today Bio

journal homepage: www.journals.elsevier.com/materials-today-bio

Tailored virus-mimicking nanoparticles mediate high transfection of pTRAIL for bystander effects in oncotherapy

Ruirong Wu [a], Xiufeng Wu [b], Lan Zhang [c], Feng Zhang [d], Yang Ding [d,*], Yong Mao [a,**], Jiang Ni [b,***]

[a] Department of Medical Oncology, Affiliated Hospital of Jiangnan University, Wuxi, 214028, China
[b] Department of Pharmacy, Affiliated Hospital of Jiangnan University, Wuxi, 214028, China
[c] Jiangnan University Medical Center, Wuxi School of Medicine, Jiangnan University, Wuxi, 214000, China
[d] State Key Laboratory of Natural Medicines, Department of Pharmaceutics, China Pharmaceutical University, Nanjing, 210009, China

ARTICLE INFO

Keywords:
Virus-mimicking nanoparticles
Tumor-targeted accumulation
ROS-Responsive burst release
TRAIL-Specific bystander effects
Safe and efficient oncotherapy

ABSTRACT

Viral vectors share unparalleled gene-transfection efficiency due to protein capsid-mediated target-cell recognition and efficient cellular translocation, but clinical applications are seriously hampered by potential biosafety issues. Herein, we develop a virus-mimicking nanoparticle to enable safe, selective, and efficient TRAIL-expressing plasmid (pTRAIL) transfection for site-specific apoptosis and bystander effects. For preparation, a reactive oxygen species (ROS)-responsive phenylboronic acid-rich quaternized polymer (CRP) is synthesized for electrostatic compression of pTRAIL and coordinative coupling for apolipoprotein A-I with iRGD peptide conjugation, which is termed as iaCRP/pTRAIL nanoparticles with "gene core-protein shell" structure. The tailored virus-mimicking nanoparticles could prevent pTRAIL payloads from serum elimination, accompanied by site-specific accumulation and penetration. After cellular internalization, ROS-triggered nanoparticles disassembly could further perform burst pTRAIL release and high TRAIL expression. Our findings confirm TRAIL-derived apoptosis and bystander effects, giving *in vivo* tumor inhibition of ~80 % and metastasis suppression of over 90 %. Collectively, the virus-mimicking strategy provides novel insights into bionic gene delivery and transfection design for efficient and safe oncotherapy.

1. Introduction

Gene therapy holds great promise for tumor treatment [1], but its clinical application has been hindered by considerable challenges in transfection [2]. Generally, viral and non-viral vectors represent two significant classes of delivery systems for packaging genetic cargo and facilitating transfection [3]. Viral vectors possess superior transgenic efficiency [4], but come with inherent drawbacks, such as immunogenicity and safety concerns related to uncontrolled replication and integration of genetic material into the host genome. Moreover, viruses are vulnerable to neutralization by natural immunoglobulin M antibodies and complement components, leading to rapid clearance by the reticuloendothelial system [5]. In contrast, non-viral vectors offer improved safety profiles but generally express significantly lower gene transfection efficiency than their viral counterparts [6]. To combine the advantages of both viral and non-viral vectors, biomimetic strategies are explored to mimic viral biostructure and transfection mechanisms for efficient and safe gene delivery [7].

In biostructure of viruses, capsid acts to protect genome from degradation, identify host cells, mediate cellular uptake, and unpackage gene in cytoplasm of host cells [8], indicating that biomimicking capsid design is the key to targeted transfection of virus-like vectors. Integrin on cytomembrane has been identified as the most important receptor for mediating virus infection [9]. Integrin $\alpha_V\beta_3$ is commonly overexpressed on tumor cell membranes, making tumors susceptible to virus transfection [10]. Therefore, modifying artificial capsids with internalizing Arg-Gly-Asp (iRGD) peptide, a targeting ligand for integrin $\alpha_V\beta_3$, could be an effective strategy for site-specific transfection in tumors [11]. In addition, utilizing endogenous components for capsid fabrication offers a promising solution for overcoming rapid clearance during circulation.

* Corresponding author.
** Corresponding author.
*** Corresponding author.
E-mail addresses: dydszyzf@163.com (Y. Ding), 9812015252@jiangnan.edu.cn (Y. Mao), nj1876348@suda.edu.cn (J. Ni).

https://doi.org/10.1016/j.mtbio.2025.101633
Received 16 November 2024; Received in revised form 18 February 2025; Accepted 2 March 2025
Available online 4 March 2025

Apolipoprotein A-I (apoA-I), the main component of natural high-density lipoprotein with high biocompatibility and biostability [12], could be a potential candidate for constructing biomimetic capsids. The active intracellular gene release is another crucial reason for the high transfection of viral vectors; and achieving this through protein structure design is challenging [13]. Polymers are capable of active and rapid gene release upon specific microenvironments inside tumor cells, offering promises in simulating intracellular gene unpackage of viruses [14]. Due to the aberrant metabolism of tumor cells, the intracellular environment significantly differs from normal tissues, including elevated levels of reactive oxygen species (ROS) ranging from 1 to 10 mM. Accordingly, ROS-responsive structures are broadly investigated in designing tumor-specific carriers [15]. ROS can also provide electrons during oxidation processes, which facilitates the neutralization of positive charges, leading to active gene release while ensuring biosafety of drug delivery systems.

Considering the druggability of therapeutic genes in oncotherapy, tumor necrosis factor-related apoptosis-inducing ligand (TRAIL) has garnered significant attention in the clinical development of targeted tumor therapy [16], given its capacity to induce apoptosis selectively in cancer cells without harming normal cells [17]. Numerous recombinant forms of TRAIL protein and TRAIL-receptor agonists, such as antibodies, have been developed and evaluated in clinical studies; however, only one recombinant TRAIL known as Aponermin® has been approved for marketing recently [18]. In clinical practice, the TRAIL drug of Aponermin® is approved to treat relapse/refractory multiple myeloma in combination with thalidomide and dexamethasone by National Medical Products Administration (NMPA). Moreover, 7 combination regimens of Aponermin® have been included in "2024 Chinese Society of Clinical Oncology (CSCO) Guidelines for Diagnosis and Treatment of Malignant Hematological Diseases". The combinative strategies may elevate the sensitivity of tumor cells to TRAIL, via upregulating DR4/5 expression and other underlying mechanisms. *In vivo,* the short half-life of TRAIL in circulation emerges as a crucial reason for the clinical failures of TRAIL drug development, which inspires orthotopic TRAIL gene expression strategy for sustaining TRAIL protein generation [19]. Moreover, continuous and high-level TRAIL generation could energize bystander effect for enhanced suppression of primary tumor and metastasis, as tumor cells with metastatic phenotype are more sensitive to TRAIL.

Herein, a virus-mimicking nanoparticle was fabricated to enable safe, selective, and efficient TRAIL-expressing plasmid (pTRAIL) transfection for tumor-targeted apoptosis (Scheme 1). Structurally, we synthesized a cationic ROS-responsive phenylboronic acid-rich quaternized polymer (CRP) with the capacity for electrostatic gene compression and coordinate protein coupling. Sequential assembly of CRP polymer with pTRAIL and iRGD peptide-modified apolipoprotein A-I (iRGD-apoA-I) generated the virus-mimicking drug delivery system (iaCRP/pTRAIL) with "gene core-protein shell" structure. Upon intravenous administration, the virus-mimicking nanoparticles could protect pTRAIL payloads during circulation, accompanied by site-specific accumulation and deep-tumor penetration via coordinately assembled iRGD-apoA-I capsid. After cellular internalization, the nanoparticles of iaCRP/pTRAIL would be disassembled by concentrated ROS for rapid pTRAIL liberation and efficient TRAIL expression. The efficient transfection of virus-mimicking nanoparticles would yield advanced tumor suppression upon apoptosis signal spreading. The virus-mimicking strategy offers novel insights into bionic drug delivery design for effective and safe oncotherapy. Compared with traditional non-viral gene carriers, the biodegradable and positive-charge-elimination polymer design could solve the contradiction between positive charge for gene compression and biosafety. Moreover, the responsive gene liberation could bring remarkable elevation in transfection efficacy. Most of the reported viral mimetics are based on polymers or inorganic materials to build core-shell structure, and the main merits are to imitate surface binding of virus and cytomembrane. The virus-mimicking strategy innovatively uses protein-peptide conjugate to build "capsid" for completely bio-shielding and targeting. Due to the responsiveness of CRP polymer, the virus-mimicking system could simulate the intracellular biological

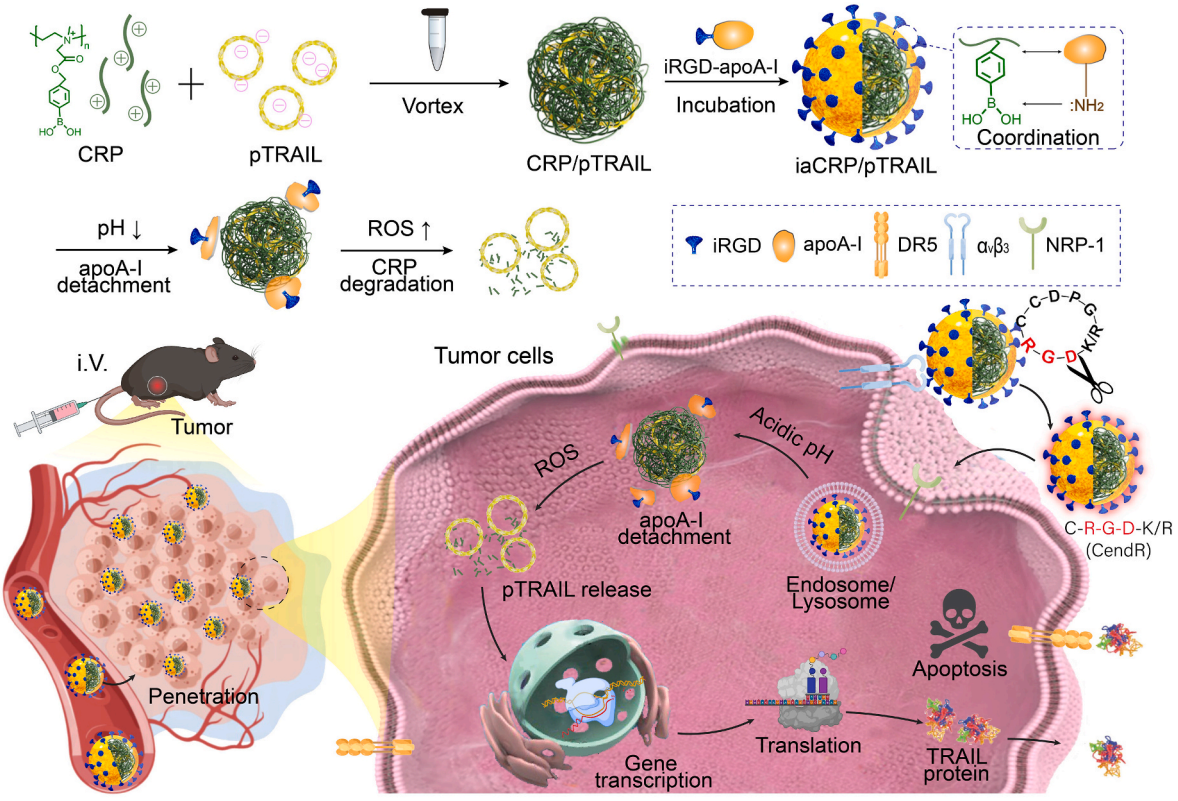

Scheme 1. Schematic illustration of the preparation, delivery, and transfection process of iaCRP/pTRAIL as the virus-mimicking nanoparticles.

processes of virus, including active detachment of capsid, and gene release for advanced transfection.

2. Materials and methods

2.1. Materials

Apolipoprotein A-I (apoA-I) was extracted from Cohn Fraction IV in our lab [20]. Sulfosuccinimidyl 4-(nmaleimidomethyl) cyclohexane-1-carboxylate (Sulfo-SMCC) was bought from Highfine Co., Ltd. (Jiangsu, China). The thiolated iRGD peptide (CRGDKGPDC) was obtained from GL Biochem Co., Ltd. (Shanghai, China). 3-Hydroxytyramine hydrochloride, dimethylsulfoxide (DMSO), 4-(bromomethyl) phenylboronic acid, 4-carboxyphenylboronic acid, potassium iodide, and polyethyleneimine (PEI) were bought from Aladdin Reagent Co., Ltd. (Shanghai, China). Sodium dodecylsulphate polyacrylamide gel electrophoresis (SDS-PAGE) gel quick preparation kit and BCA protein detection kit were bought from Beyotime Biotechnology Co., Ltd. (Shanghai, China). 3-(4,5-Dimethylthiazol-2-yl)-2,5-diphenyltetrazolium bromide (MTT) was bought from Yifeixue Bio-Tech (Jiangsu, China). 4,6-Diamidino-2-phenylindole (DAPI), formaldehyde solution, chloroacetic acid, formic acid, and dialysis bag (MWCO 7000 Da) were bought from Yeasen Bio-Tech (Shanghai, China). Annexin V-FITC/propidium iodide (PI) Apoptosis Detection Kit was bought from Vazyme Biotech Co., Ltd. (Jiangsu, China). Label IT® Tracker TM Intracellular Nucleic Acid Localization Kit was purchased from Mirus Bio Co., Ltd. (Beijing, China). TIANprep Mini Plasmid Kit was purchased from TIANGEN Biotech Co., Ltd. (Beijing, China). Tumor necrosis factor-related apoptosis-inducing ligand (TRAIL)-expressing plasmid (pTRAIL) was constructed by General Biol Co., Ltd. (Jiangsu, China).

2.2. Synthesis and characterization of polymers

Cationic reactive oxygen species (ROS)-responsive phenylboronic acid-rich quaternized polymer (CRP) was prepared via a three-step method. The tertiary amination product of PEI (t-PEI) was obtained by Eschweiler-Clarke reaction. Briefly, 1 g of PEI was dissolved in 5 g of formic acid in ice bath, followed by a slow addition of 6 mL formaldehyde solution, and then heated up at 95 °C for 8 h in oil bath. The solvent of formic acid and formaldehyde was removed by a rotary evaporator to obtain the t-PEI product. To obtain the quaternary product of PEI (qua-PEI), 945 mg of chloroacetic acid was dispersed in water and followed by the addition of sodium hydroxide solution to adjust pH to 9 to yield sodium chloroacetic acid solution. 0.1 g of t-PEI was added to sodium chloroacetic acid solution and stirred at 50 °C for 12 h, followed by dialysis in water for 48 h and lyophilization to produce qua-PEI. CRP polymer was further prepared via esterification reaction. 30 mg of qua-PEI polymer and 4-bromomethyl phenylboronic acid were dissolved in DMSO at a molar ratio of 1: 1.5 and stirred for 24 h in the presence of sodium carbonate and potassium iodide. The above products were characterized by ^{1}H nuclear magnetic resonance (^{1}H NMR) and Fourier transform infrared spectroscopy (FTIR). Cationic unresponsive phenylboronic acid-rich polymer (CPP) was synthesized as control by two steps. The phenylboronic acid groups were conjugated on PEI polymer via amidation, followed by quaternization with methyl iodide.

2.3. Preparation and characterization of iaCRP/pTRAIL nanoparticles

Polymer solution of CRP was mixed with pTRAIL solution dropwise upon vortex to prepare CRP/pTRAIL nanoparticles. The nanoparticles prepared at desired N/P ratios (0, 0.5, 1, 2, 3, 4, 5, 6) were analyzed by gel retardation electrophoresis to evaluate gene compression capacity of CRP polymer, using free pTRAIL as a negative control. iRGD peptide was conjugated on apoA-I using sulfo-SMCC as a linker to synthesize iRGD peptide modified apoA-I (iRGD-apoA-I). In brief, 0.33 mg of sulfo-SMCC and 2.5 mg of apoA-I were dissolved in 1 mL of phosphate buffer saline (PBS, 0.1 M, pH 7.4), followed by stirring at 25 °C for 3.5 h. 0.2 mL of iRGD peptide solution (10 mg/mL) was dropped into the above mixture and stirred for 3 h. The reaction mixture was dialyzed with a dialysis bag (MWCO 7000 Da) against water for 24 h, followed by lyophilization to yield iRGD-apoA-I.

pH value of CRP/pTRAIL nanoparticles solution (40 μg/mL) was adjusted to ~8.0 with sodium bicarbonate solution. Thereafter, CRP/pTRAIL nanoparticles were incubated with iRGD-apoA-I protein for 12 h under slow stirring to obtain a virus-mimicking nanoparticle termed as iaCRP/pTRAIL. Particle size, polydispersity index (PDI), and zeta potential of CRP/pTRAIL and iaCRP/pTRAIL nanoparticles were measured by dynamic light scattering (DLS, Zetasizer Nano ZS, Malvern, UK). Moreover, morphological characteristics of the nanoparticles were observed using a transmission electron microscope (TEM, HT7800, HITACHI, Japan). The coordinative binding between CRP polymer and iRGD-apoA-I was detected by X-ray photoelectron spectroscopy (XPS, ESCALAB, Thermo Scientific, USA) analysis. CRP/pTRAIL and iaCRP/pTRAIL nanoparticles solutions were lyophilized to corresponding powders and subjected to XPS analysis. The storage stability of iaCRP/pTRAIL nanoparticles was evaluated by storing the nanoparticles at 4 °C for 25 days, with diameter and PDI measured via DLS. Serum stability of iaCRP/pTRAIL nanoparticles was further assessed by incubating nanoparticles products in 20 % fetal bovine serum (FBS). Diameter and PDI were measured at predominated time intervals.

2.4. ROS-responsive gene release

To investigate ROS-responsive gene release of CRP polymer, iaCRP/pTRAIL nanoparticles were incubated in different concentrations of H_2O_2 solution (0, 0.1, 0.5, 1, 2.5, 5 mM) for 12 h. The released pTRAIL was detected using an agarose gel electrophoresis assay. Furthermore, pTRAIL release profile of iaCRP/pTRAIL nanoparticles was investigated via incubation in different medium of pH 5.0 + 0.1 mM H_2O_2, pH 7.4 + 0.1 mM H_2O_2, pH 5.0 + 0.001 mM H_2O_2. Nanoparticles in the medium were removed via ultracentrifugation, and the released pTRAIL in each group was measured with NanoDrop microanalyze (K5600/C, Kaiao Technology, China) at predesigned time intervals of 0, 0.5, 1, 2, 4, 6, 8, 12, 18, 24, 36, and 48 h.

2.5. Cellular uptake and intracellular trafficking

The mouse mammary carcinoma cell lines of E0771 and 4T1, and Chang Liver cell line were purchased from Shanghai Institute of Biochemistry and Cell Biology, Chinese Academy of Sciences, Shanghai, China. The cellular uptake was qualitatively observed and quantitatively determined by confocal laser scanning microscopy (CLSM, LSM700, Zeiss, Germany) and flow cytometry (FCM, FACSMelody, BD Biosciences, USA), respectively. In brief, pTRAIL was labeled with Cy5 (Cy5-pTRAIL) using Label IT® Tracker TM Intracellular Nucleic Acid Localization Kit, and Cy5-pTRAIL was used to prepare Cy5-labeled nanoparticles. Non-iRGD-decorated apoA-I was used to fabricate aCRP/Cy5-pTRAIL nanoparticles, and bull serum albumin (BSA) was employed to substitute iRGD-apoA-I to construct bCRP/Cy5-pTRAIL nanoparticles as control. To compare the selectivity of iaCRP/Cy5-pTRAIL between tumor cells and normal cells, Chang Liver cells were used as control group.

For CLSM analysis, E0771 cells were seeded in glass-bottom dishes (8×10^4 cells per dish) and cultured at 37 °C for 24 h iaCRP/Cy5-pTRAIL, aCRP/Cy5-pTRAIL, and bCRP/Cy5-pTRAIL nanoparticles were dispersed in serum-free medium at Cy5-pTRAIL concentration of 1 μg/mL and inculcated with E0771 cells for 2, 4, 8, and 12 h. The cells were fixed with 4 % paraformaldehyde solution for 20 min at each time interval, followed by nuclei staining with 2 μg/mL DAPI for 8 min. The cellular internalization and intracellular distribution of the nanoparticles were observed under CLSM. As for FCM samples, cells were seeded in 24-well plates (8×10^4 cells per well) and cultured at 37 °C for

24 h. The cells were treated with iaCRP/Cy5-pTRAIL, aCRP/Cy5-pTRAIL, and bCRP/Cy5-pTRAIL nanoparticles at Cy5-pTRAIL concentration of 1 μg/mL for 2, 4, 8, and 12 h. At each time interval, cells were collected via digestion and centrifugation and subjected to flow cytometry analysis to quantitatively determine the cellular uptake efficiency of the nanoparticles.

2.6. Intracellular pTRAIL liberation

To investigate intracellular pTRAIL liberation, carboxyfluorescein (FAM)-labeled CRP (FCRP) and CPP (FCPP) was synthesized. In brief, PEI polymer was firstly conjugated with FAM moieties via amidation to generate FAM-PEI polymer. Thereafter, FAM-PEI polymer was used to synthesize FCRP and FCPP polymer following the steps described above of CRP and CPP synthesis. The FAM-labeled polymers and Cy5-pTRAIL were employed to fabricate dual-fluorescence-labeled nanoparticles of iaFCRP/Cy5-pTRAIL and iaFCPP/Cy5-pTRAIL. E0771 cells were plated onto glass-bottom dishes (8×10^4 cells per dish) and cultured for 24 h. The medium was replaced with serum-free medium containing iaFCRP/Cy5-pTRAIL and iaFCPP/Cy5-pTRAIL nanoparticles, respectively. The cells were co-incubated with the nanoparticles for 4 h, and the nanoparticle-containing medium was replaced with fresh medium. At 0.5, 1, 3, and 6 h post nanoparticles withdrawal, the cells were washed three times and stained with DAPI before observation by CLSM. The colocalization of FAM-labeled polymers and Cy5-pTRAIL was analyzed using Image J.

2.7. Gene transfection efficiency evaluation

To evaluate transfection efficiency of virus-mimicking nanoparticles, BSA was used to fabricate the protein corona to give bCRP/pTRAIL nanoparticles, and non-iRGD-decorated apoA-I was used to fabricate aCRP/pTRAIL nanoparticles, and unresponsive CPP polymer was used to prepare iaCPP/pTRAIL nanoparticles as control groups. E0771 cells were seeded in 24-well plates at a density of 8×10^4 cells per well and cultured for 24 h. Thereafter, the culture medium was replaced with serum-free medium containing bCRP/pTRAIL, aCRP/pTRAIL, iaCPP/pTRAIL, and iaCRP/pTRAIL solutions at pTRAIL concentration of 1 μg/mL. PBS of the same volume of nanoparticles was used as negative control. After incubation for 8 h, the nanoparticle-containing medium was discarded, and fresh medium supplemented with 10 % FBS was added to each well, followed by further culture for another 40 h. To better demonstrate the tumor selectivity of the virus-mimicking nanoparticles, iaCRP/pTRAIL was used to treat E0771 cells, 4T1 cells and Chang Liver cells. Particularly, N-acetylcysteine (NAC) was used to eliminate ROS in E0771 cells and 4T1 cells before treatment as control, and H_2O_2 was used to treat Chang Liver cells before treatment to simulate high ROS level as control. TRAIL expression was measured by an inverted fluorescence microscope (Eclipse Ts2-FL, Nikon Precision Inc., CA, USA) and FCM, as TRAIL was fused with enhanced green fluorescent protein (EGFP).

2.8. Cytotoxicity and bystander effect study

Cytotoxicity of virus-mimicking nanoparticles was evaluated using an MTT assay. The materials and preparations of CRP, CPP, aCRP/ncDNA, bCRP/ncDNA, iaCPP/ncDNA and iaCRP/ncDNA were subjected to MTT assay against E0771 cells and Chang Liver cells for biosafety testing. E0771 cells were seeded in 96-well plates (5×10^3 cells per well). After culture for 24 h, the medium in each well was replaced with serum-free medium containing different nanoparticles, including aCRP/pTRAIL, bCRP/pTRAIL, iaCRP/pTRAIL, and iaCPP/pTRAIL. To better demonstrate tumor selectivity of the virus-mimicking nanoparticles, iaCRP/pTRAIL was applied to treating E0771 cells and Chang Liver cells. Particularly, N-acetylcysteine (NAC) was used to eliminate ROS in E0771 cells before treatment as control, and H_2O_2 was used to treat Chang Liver cells before treatment to simulate high ROS level as control. After incubation for 8 h, the nanoparticles-containing medium was replaced with a fresh medium containing 10 % FBS. After culture for another 40 h, 20 μL of MTT (5 mg/mL) solution was added to each well and the cells were cultured incubated for 4 h. The medium was discarded, and 100 μL of DMSO was added to dissolve formazan crystals in living cells. At the same time, blank control and negative control groups were set. The absorbance at 570 nm was measured using a universal microplate reader (EL800, BIO-TEK Instruments Inc., USA), and the percentage of cell viability was calculated according to formula (1).

$$\text{Cell viability} = \frac{A_{\text{sample}} - A_{\text{blank}}}{A_{\text{control}} - A_{\text{blank}}} \times 100\% \quad (1)$$

The bystander effect of TRAIL expression was further investigated. In brief, E0771 cells were inoculated in a 6-well plate at a density of 1×10^5 cells per well. When cells grew to 80 % fusion, medium containing aCRP/pTRAIL, bCRP/pTRAIL, iaCRP/pTRAIL, and iaCPP/pTRAIL nanoparticles was added, followed by incubation for 8 h. The nanoparticles-containing medium was then replaced with a complete medium to culture cells for another 40 h. The supernatant of each group was collected and used to treat E0771 cells for 24 h. The supernatant-treated cells were collected, and apoptosis was detected using the Annexin V-FITC/PI cell apoptosis kit.

2.9. Animals and tumor model

Female C57BL/6 mice (6–8 weeks, 18–22 g) were purchased from Qing Longshan Laboratory Animal Center (Nanjing, China). All animals were pathogen-free and allowed to access food and water freely. The animal experiment protocol was approved by China Pharmaceutical University Ethics Committee and followed the National Institute of Health Guide for the Care and Use of Laboratory Animals. To establish the orthotopic breast cancer model, 5×10^5 of E0771 cells were inoculated in the left side of the 4th pair mammary fat pads of female C57 mice. The tumor volume was measured by a fine caliper, and the tumor volume (V) was calculated according to formula (2), where L and W represented the length and width of tumors, respectively.

$$V = \frac{L \times W^2}{2} \quad (2)$$

2.10. Safety profiles

A hemolysis examination was conducted to evaluate whether virus-mimicking nanoparticles were safe for intravenous injection. The red blood cells (RBC) were taken from a healthy rabbit and diluted with saline to produce RBC suspension of 2 %. iaCRP/pTRAIL and CRP/pTRAIL nanoparticles were diluted with saline to generate various pTRAIL concentrations. Thereafter, RBC suspension was mixed with iaCRP/pTRAIL and CRP/pTRAIL solution at the same volume where the final pTRAIL concentrations were 0, 0.2, 0.4, 0.6, 0.8, 1, 2, 3, 4, and 5 μg/mL. The mixtures were incubated at 37 °C for 1 h, and then all the samples were centrifuged at 3000 rpm for 5 min. The absorbance of supernatants at 540 nm was measured using a microplate reader. 0 % and 100 % hemolysis were obtained from red blood cells suspended in normal saline and distilled water, respectively. The percentage of hemolysis was determined according to formula (3).

$$\text{Hemolysis}\ (\%) = \frac{A_{\text{sample}} - A_{0\%}}{A_{100\%} - A_{0\%}} \times 100\% \quad (3)$$

To investigate *in vivo* safety of virus-mimicking nanoparticles, healthy female C57BL/6 mice aged 6–8 weeks were injected with iaCRP/pTRAIL nanoparticles intravenously at a pTRAIL dosage of 1 mg/kg, and PBS was used as negative control. Blood samples and main organs (heart, liver, spleen, lung, and kidney) were collected from each group. Serum samples were prepared by centrifugation at 1000*g* for 10

min after complete coagulation of blood at room temperature. Serum was sampled to analyze heart, liver, and kidney functions by detecting creatine kinase (CK), aspartate aminotransferase (AST), alanine aminotransferase (ALT), alkaline phosphatase (ALP), blood urea nitrogen (BUN), and creatinine (CRE). The main organs of each group were fixed in 4 % formaldehyde solution for H&E staining.

2.11. In vivo imaging and biodistribution analysis

To monitor *in vivo* biodistribution of virus-mimicking nanoparticles, Cy5-labeled pTRAIL was used to prepare Cy5-labeled nanoparticles of iaCRP/Cy5-pTRAIL, aCRP/Cy5-pTRAIL and bCRP/Cy5-pTRAIL. After intravenous administration at Cy5-pTRAIL dosage of 1 mg/kg, the biodistribution of nanoparticles in tumor-bearing mice was analyzed by an *in vivo* imaging system (IVIS Spectrum, Caliper LifeSciences, PerkinElmer, Inc., USA) within 24 h at *Ex* = 650 nm and *Em* = 670 nm. Thereafter, mice were euthanized, and main organs (heart, liver, spleen, lung, and kidney) and tumors were excised for *ex vivo* imaging. The fluorescence intensities were analyzed using Image Lab Software. The isolated tumor tissues were embedded in a tissue tissue-freezing medium and quickly frozen at −20 °C. Then, the tumor tissues were sliced using Leica CM Frozen microtome, followed by DAPI (1 μg/mL) staining. The fluorescence distribution of Cy5-labeled nanoparticles was observed using CLSM.

2.12. In vivo anti-tumor efficacy

Tumor-bearing mice were divided into 5 groups randomly (n = 8) when tumor volume reached 200 mm^3. The mice were injected intravenously with saline, aCRP/pTRAIL, bCRP/pTRAIL, iaCPP/pTRAIL, and iaCRP/pTRAIL every three days at a pTRAIL dosage of 1 mg/kg. The tumor volume and body weights of each mouse were measured using an electronic digital caliper and electronic scales, respectively, every three days during the treatment. Three mice in each group were sacrificed at 18 d after the first administration, and tumor tissues were dissected and separated from the mice. Tumors in each group were weighed and then subjected to western blot analysis of TRAIL, H&E staining, TUNEL staining, and immunohistochemical analysis. The remaining mice were kept under normal feeding conditions, and the survival of each group was observed. At the end of the survival investigation, the remaining mice in each group were euthanized, and intact lungs were collected. Bouin's fixation showed metastatic nodules, and the number of metastasis nodules was counted. The lungs were further slice for internal nodule evaluation.

2.13. In vivo TRAIL bystander effect

To evaluate the *in vivo* bystander effect of TRAIL therapy, TRAIL knockout C57BL/6 mice were introduced, and the mice were used to establish lung metastasis model of breast cancer. 1×10^5 luciferase-labeled E0771 cells (E0771-Luc) were injected intravenously into TRAIL knockout C57BL/6 mice, and lung metastasis formation was monitored via bioluminescence. E0771 cells were treated with virus-mimicking nanoparticles *in vitro*, and the corresponding supernatant was collected and concentrated via ultrafiltration. Different groups' supernatant was administered via vein once a day for 5 days. The lungs of mice were dissected 1 h after the last administration. Metastatic nodules on the lungs were analyzed via Bouin's fixation, and the concentration of TRAIL protein in the lungs was detected using an enzyme linked immunosorbent assay (ELISA) kit.

2.14. Statistical analysis

All data were presented as mean ± S.D. Statistical analysis was evaluated by using the two-tailed unpaired Student's t-test. The value of $^*P < 0.05$, $^{**}P < 0.01$, and $^{***}P < 0.001$ were regarded as statistically significant.

3. Results and discussions

In the present study, a virus-mimicking gene delivery system was developed for tumor-targeted apoptosis and bystander effects. A novel protein-polymer hybrid artificial capsid was constructed to simulate cellular internalization, and automatic gene unpackage of the virus. The virus-mimicking nanoparticles demonstrated advanced transfection efficiency and significant biosafety both *in vitro* and *in vivo*. TRAIL gene was employed as a therapeutic agent and yielded efficient tumor suppression, benefiting from high tumor-targeted transfection of virus-mimicking nanoparticles. Moreover, the high transfection amplified bystander effects of TRAIL therapy, contributing to metastasis blockage and elimination. Therefore, the virus-mimicking nanoparticles provide a novel option for treating localized and metastatic cancer.

3.1. Preparation and characterization of iaCRP/pTRAIL nanoparticles

Cationic reactive oxygen species (ROS)-responsive phenylboronic acid (PBA)-rich quaternized polymer (CRP) was synthesized from polyethyleneimine (PEI) via Eschweiler-Clarke reaction, quaternization, and esterification (Fig. S1), and cationic non-responsive PBA-rich polymer (CPP) was designed and synthesized as control (Fig. S2). The chemical structure of CRP and CPP polymer was characterized by ^1H nuclear magnetic resonance (^1H NMR) and Fourier transform infrared spectroscopy (FTIR) spectra (Figs. S3–4). According to ^1H NMR spectra, a single peak at δ 3.2 ppm was attributed to the induced methyl group by Eschweiler-Clarke reaction. The disappearance of N-H peak at δ 2.7 ppm indicated the formation of a quaternary ammonium structure. The chemical shift of the alkyl peak was increased due to the electron-withdrawing effect from the generated quaternary ammonium. The presence of new peaks at δ 7–8 ppm was attributed to the benzene ring, which could confirm the conjugation of PBA group. As for CPP polymer, the characteristic peak at δ 8.1 was attributed to the amide structure, and peaks at δ 7–8 ppm were attributed to the benzene ring. The results confirmed PBA group conjugation via amidation. Moreover, alkyl groups of CPP polymer shared a chemical shift similar to that of CRP polymer due to the quaternary ammonium structure. In FTIR spectra, the characteristic peak at 1726 cm^{-1} in CRP polymer and characteristic peak at 1650 cm^{-1} in CPP polymer were attributed to the stretching vibration of the ester bond/amide group, respectively. Collectively, the results could validate the successful synthesis of CRP and CPP polymers.

Tumor necrosis factor-related apoptosis-inducing ligand (TRAIL)-expressing plasmid (pTRAIL) was constructed by inserting TRAIL gene sequence into pcDNA3.1(+) plasmid vector, where TRAIL was fused with enhanced green fluorescent protein (EGFP) as a reporter (Fig. S5). pTRAIL was transformed into *E. coli* DH5α, and amplified via bacterial culture. Thereafter, pTRAIL was extracted and purified using the TIANprep Mini Plasmid Kit for further nanoparticles fabrication. For virus-mimicking nanoparticles preparation, pTRAIL was compressed by CRP polymer upon vortex to form CRP/pTRAIL nanoparticles. Thereafter, iRGD-apoA-I corona was decorated via coordination conjunction to yield iaCRP/pTRAIL nanoparticles (Fig. 1A). Gel electrophoresis indicated that CRP polymer could completely compress pTRAIL at a N/P ratio of 1: 1 (Fig. S6). The formulation of CRP/pTRAIL nanoparticles was further screened by adjusting N/P ratio, with diameter, polydispersity index, and zeta potential monitored at each N/P ratio (Fig. S7). When N/P over 4, the particle size, polydispersity index and zeta potential of CRP/pTRAIL performed no significant variations. Therefore, N/P ratio of 4:1 was chosen for further construction of the virus-mimicking nanoparticles. The optimized CRP/pTRAIL nanoparticles gave a diameter of (49.3 ± 1.9) nm with polydispersity index (PDI) of 0.17 ± 0.03. Transmission electron microscope (TEM) image further suggested a spherical structure and uniform distribution of CRP/pTRAIL nanoparticles (Fig. 1B). Moreover, abundant PBA groups could endow CRP

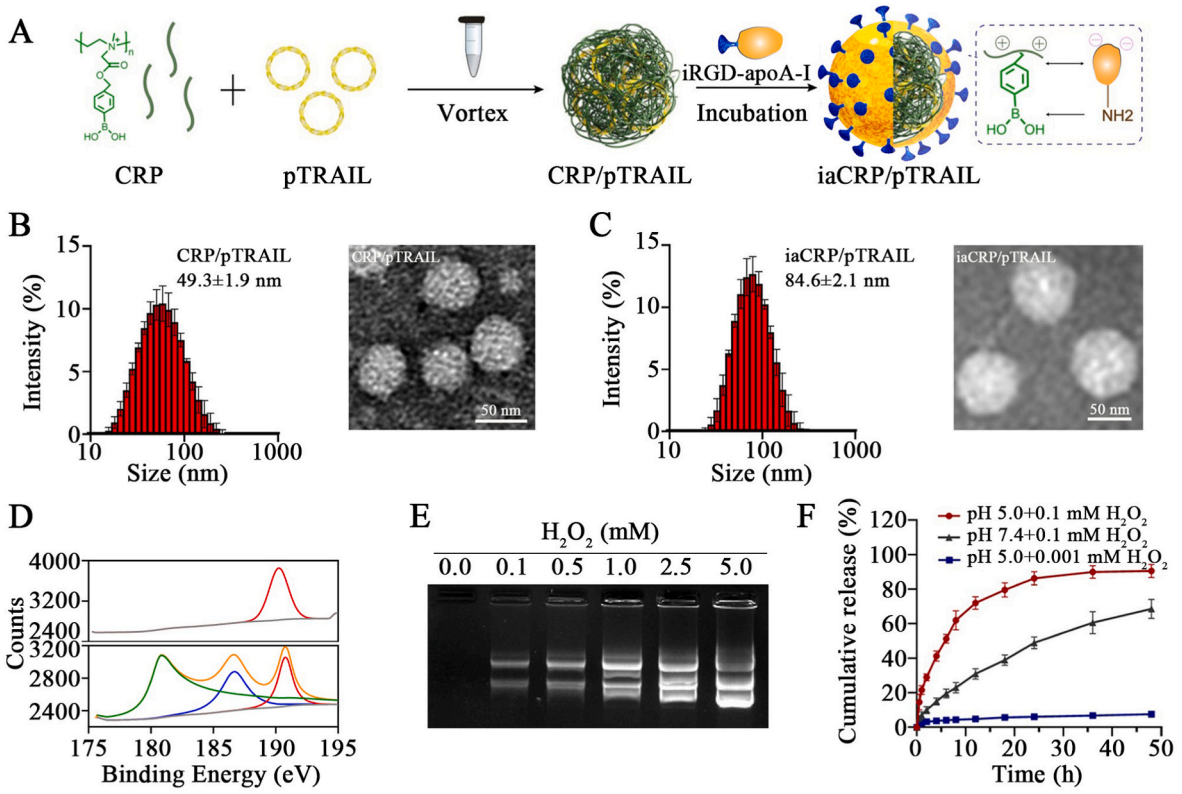

Fig. 1. Preparation and characterization of the virus-mimicking nanoparticles of iaCRP/pTRAIL. (A) Schematic illustration of iaCRP/pTRAIL nanoparticles preparation. (B) Particle size distribution and corresponding TEM image of CRP/pTRAIL nanoparticles. (C) Particle size distribution and corresponding TEM image of iaCRP/pTRAIL nanoparticles. (D) XPS spectra of CRP/pTRAIL and iaCRP/pTRAIL nanoparticles. (E) Gel retardation analysis of pTRAIL released from iaCRP/pTRAIL nanoparticles after incubation in H_2O_2 solution at different concentrations. (F) *In vitro* release behavior of pTRAIL from iaCRP/pTRAIL nanoparticles at various pH values and H_2O_2 concentrations. Results were presented as mean ± S.D. (n = 3).

polymer with intense affinity to proteins via coordination between nitrogen (N) and boron (B). Therefore, iRGD-apoA-I corona was attached onto surface of nCRP/pTRAIL nanoparticles via coordinative binding. The ratio between iRGD-apoA-I and pTRAIL was screened using diameter, polydispersity index, and zeta potential as indicators (Fig. S8). The optimized iaCRP/pTRAIL diameter was (84.6 ± 2.1) nm with spherical and uniform nanostructure (Fig. 1C). In X-ray photoelectron spectroscopy (XPS) analysis, splitting of the binding energy peak for boron could be observed when CRP polymer interacted with iRGD-apoA-I, confirming coordinative protein binding (Fig. 1D). The long-term storage and serum stability studies (Fig. S9) showed high physical and biochemical stability of the virus-mimicking nanoparticles. The results indicated that the hybrid capsid of iRGD-apoA-I and CRP polymer could effectively hinder nonspecific protein absorption blood circulation and significantly improve the stability of the nanodrug delivery system.

3.2. ROS-responsive gene release pattern

The efficient liberation of genes inside tumor cells is the key to performing high transfection and advanced curative effects. The cationic CRP polymer could be oxidized by ROS, where one oxygen atom is inserted between boron atom and benzene ring. The generated intermediate product is extremely unstable, and could be swiftly hydrolyzed into zwitterionic polymer, phydroxybenzyl alcohol (HMP), and boric acid upon molecular structure rearrangement (Fig. S10). The electroneutral zwitterionic polymer had no interactions with negatively charged TRAIL-expressing plasmid (pTRAIL), which could facilitate swift and complete release of pTRAIL. To verify ROS response of CRP polymer, CRP/pTRAIL nanoparticles were incubated in different concentrations of H_2O_2 solution, and pTRAIL release was detected via agarose gel electrophoresis. As illustrated in Fig. 1E, obvious band of released pTRAIL could be observed when H_2O_2 concentration was over 0.1 mM, indicating ROS responsiveness of CRP polymer. Furthermore, the release profiles of pTRAIL from virus-mimicking nanoparticles were investigated at different pH values and H_2O_2 concentrations (Fig. 1F). At ROS level in normal cells (0.001 mM) [21], no significant pTRAIL release was detected, and cumulative release rate in 48 h was less than 8 %. At ROS level in tumor cells (0.1 mM) and pH value of 5.0 [21], pTRAIL could be dissociated from carriers rapidly, and the cumulative release rate reached 92 % in 48 h. The results suggested tumor cell-specific gene release of virus-mimicking nanoparticles, which could ensure the biosafety of nanoparticles administration.

3.3. Cellular uptake and intracellular trafficking

The efficient cell uptake and rapid intracellular release of drug system are the prerequisites for antitumor efficacy. Bull serum albumin (BSA) was introduced to fabricate bCRP/pTRAIL nanoparticles by substituting iRGD-apoA-I. Cy5-labeled pTRAIL (Cy5-pTRAIL) was used to prepare fluorescence-labeled nanoparticles. As shown in Fig. 2A, quantitative flow cytometry analysis showed that uptake of Cy5-labled iaCRP/Cy5-pTRAIL nanoparticles by E0771 cells was saturated at 8 h, and no significant change was observed in uptake efficiency at 12 h. Thereafter, cellular uptake of Cy5-labled nanoparticles by E0771 cells was evaluated at 8 h by fluorescence imaging and cytometry analysis (Fig. 2B and C). The results indicated that iaCRP/Cy5-pTRAIL nanoparticles gave significantly higher uptake efficiency than aCRP/Cy5-pTRAIL group due to the transmembrane promoting effect of iRGD tumor penetrating peptide via binding to neuropilin-1 (NRP-1) receptor. Moreover, the cellular uptake efficiency of aCRP/Cy5-pTRAIL treatment was significantly higher than that of bCRP/pTRAIL group, suggesting cellular uptake promotion of apoA-I by binding to scavenger receptor

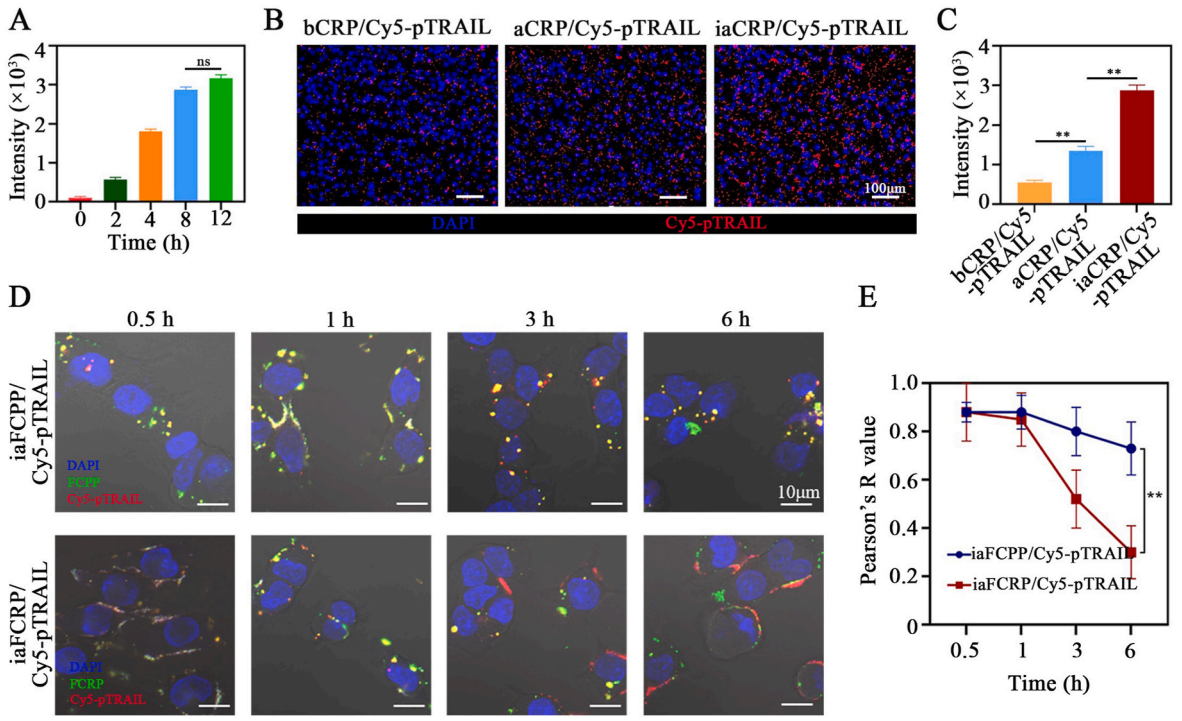

Fig. 2. Intracellular delivery of virus-mimicking nanoparticles. (A) Quantitative flow cytometry analysis on cellular uptake of iaCRP/Cy5-pTRAIL after incubation for 2, 4, 8, and 12 h. (B) E0771 cell uptake of bCRP/Cy5-pTRAIL, aCRP/Cy5-pTRAIL, and iaCRP/Cy5-pTRAIL nanoparticles after co-incubation for 8 h. (C) Flow cytometry analysis and quantification of fluorescence intensity of the cellular uptake of various nanoparticles. (D) Observation of gene release of dual fluorescence-labeled iaFCRP/Cy5-pTRAIL and iaCPP/Cy5-pTRAIL nanoparticles in E0771 cells at 0.5, 1, 3, and 6 h post withdrawal of the nanoparticles. (E) Pearson's R value of green (FAM-labeled polymers) and red fluorescence (Cy5-pTRAIL) in E0771 cells at 0.5, 1, 3, and 6 h. Results were presented as mean ± S.D. (n = 3), **P < 0.01.

class B type I (SR-BI) receptors on tumor cells. The cellular uptake of iaCRP/pTRAIL nanoparticles against E0771 cells, 4T1 cells and Chang Liver cells was further investigated. As shown in Fig. S11, breast cancer cells of E0771 cells and 4T1 cells performed significantly higher cellular uptake than Chang Liver cells, indicating potential tumor selectivity and biosafety for *in vivo* applications.

Rapid gene liberation is crucial to guarantee high transfection efficacy. Thus, pTRAIL unpackage in tumor cells was further investigated by fluorescence colocalization of polymers and pTRAIL. Cy5-pTRAIL and carboxyfluorescein (FAM)-labeled CRP (FCRP) and CPP (FCPP) polymers were used to fabricate dual-fluorescence labeled nanoparticles of iaFCRP/Cy5-pTRAIL and non-responsive iaFCPP/Cy5-pTRAIL. Fluorescence distribution of dual-labeled nanoparticles in E0771 cells was shown in Fig. 2D. E0771 cells were incubated with iaFCRP/Cy5-pTRAIL and iaFCPP/Cy5-pTRAIL for 4 h, followed by withdrawal of nanoparticles. At 0.5 h and 1 h after nanoparticles withdrawal, green fluorescence of FAM-CRP polymer and red fluorescence of Cy5-pTRAIL were co-located and demonstrated yellow fluorescence. With the extension of period, green and red fluorescence were separated gradually, giving complete dissociation at 6 h. As shown in Fig. 2E, Pearson's colocalization correlation coefficient (R) of green (FAM-labeled polymers) and red fluorescence (Cy5-pTRAIL) in iaFCRP/Cy5-pTRAIL group kept decreasing gradually, and shared a low Pearson's R value of 0.30 at 6 h. However, in the non-responsive group of iaFCPP/Cy5-pTRAIL, most of the red and green fluorescence of iaFCPP/Cy5-pTRAIL kept overlapped into yellow fluorescence, yielding a high Pearson's R value of 0.83 at 6 h. Accordingly, CRP polymer was sensitive to ROS-concentrated environment in tumor cells, and gene release was swift to enable high transfection. However, compared with CRP polymer, PBA groups in CPP structure were grafted by amide bond, and did not have ability of ROS response and charge transfer, leading to deficient gene liberation.

3.4. In vitro gene transfection efficiency

Viral vectors share incomparable transfection efficiency due to protein capsid-mediated recognition and translocation on target cells and following active intracellular gene liberation. As shown in Fig. 3A and B and Fig. S12, TRAIL expression of iaCRP/pTRAIL was observed by fluorescent inverted microscope at 48 h after administration. Compared with PBS control groups, pTRAIL-loading groups could express TRAIL-EGFP fusion green fluorescent protein effectively. The fluorescence intensity of aCRP/pTRAIL group was slightly higher than that of bCRP/pTRAIL, indicating that apoA-I protein itself had tumor-targeting effect by binding to SR-BI receptors. Notably, iaCRP/pTRAIL group shared the highest EGFP fluorescence intensity compared with other groups. To better demonstrate tumor selectivity of the virus-mimicking nanoparticles, TRAIL expression of virus-mimicking nanoparticles was estimated in E0771 cells, 4T1 cells, and Chang Liver cells. E0771 cells and 4T1 cells were pre-treated with NAC to eliminate ROS as control. Chang Liver cells were pretreated with H_2O_2 to simulate high ROS concentration as control. As shown in Fig. S13, after iaCRP/pTRAIL treatment, E0771 cells and 4T1 cells gave high TRAIL expression, but TRAIL expression level was significantly decreased when ROS was eliminated via N-acetylcysteine (NAC) treatment. In Chang Liver cells, the virus-mimicking nanoparticles only induced considerably low TRAIL expressing. However, TRAIL expression in Chang Liver cells was notably increased when the cells were pretreated with H_2O_2. The results suggested that the enhanced cellular uptake from iRGD-apoA-I capsid, and ROS-responsive gene liberation were crucial to advance transfection efficiency of the virus-mimicking nanoparticles.

3.5. Cytotoxicity and TRAIL bystander effect study

After confirmation that iaCRP/pTRAIL nanoparticles treatment can effectively express TRAIL protein, apoptosis-inducing effect of

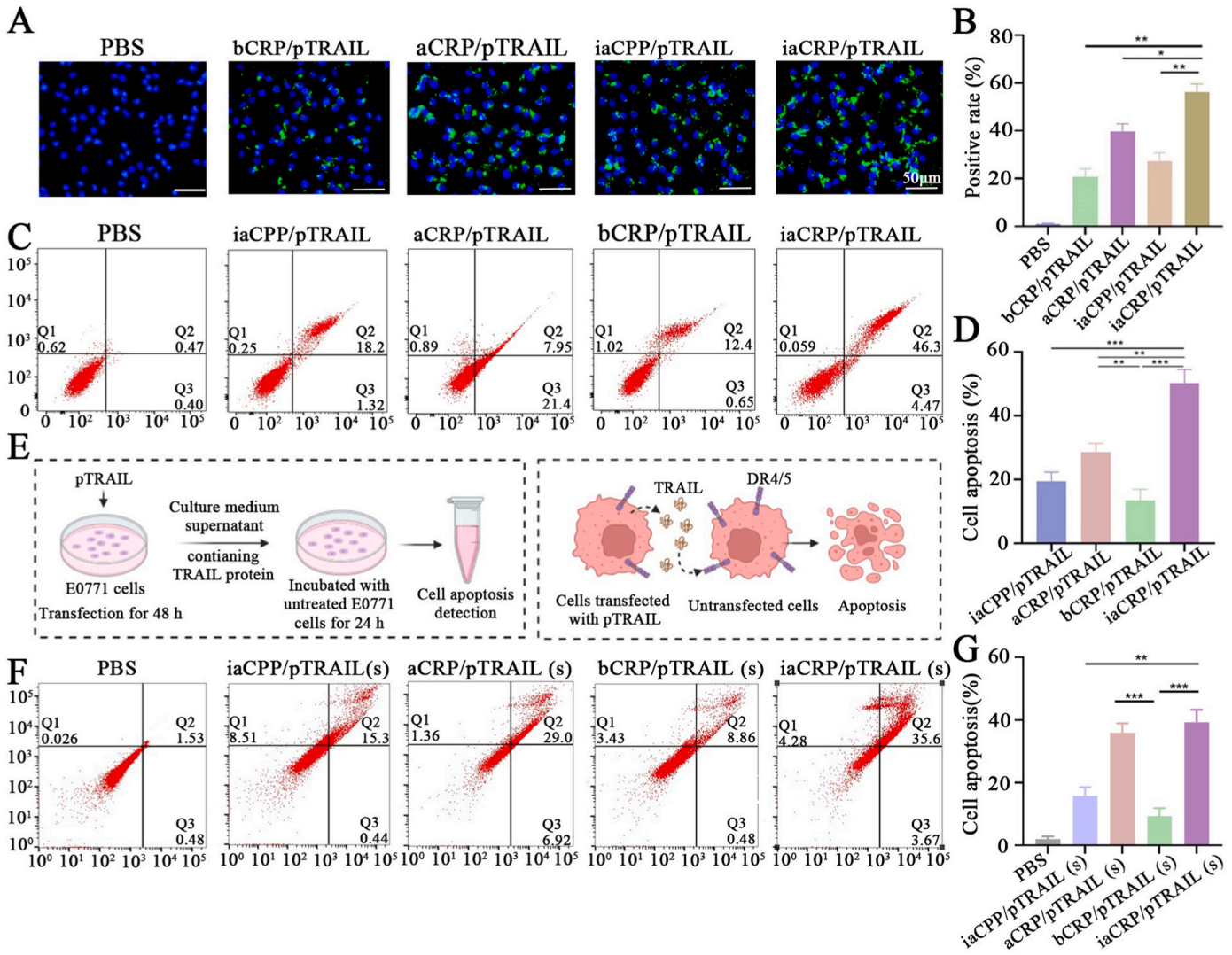

Fig. 3. *In vitro* anti-tumor efficacy and bystander effect of iaCRP/pTRAIL nanoparticles. (A) Transfection effect and expression efficiency of TRAIL-EGFP plasmid with different nanoparticles. DAPI was shown in blue and EGFP was shown in green. (B) Quantitative flow cytometric analysis of TRAIL-EGFP plasmid after transfection by different nanoparticles. (C) Apoptosis analysis of E0771 cells treated with different nanoparticles by flow cytometer. Cells treated with PBS were used as a control group. (D) Quantitative analysis of cell apoptosis induced by different nanoparticles. Cells treated with PBS were used as a control group. (E) Schematic illustration of bystander effect of TRAIL therapy. (F) Bystander effect analysis of different nanoparticles by flow cytometry after being treated with TRAIL-containing supernatant for 24 h. (G) Quantitative analysis of bystander apoptosis induced by different nanoparticles. Results were presented as mean ± S.D. (n = 3), *P < 0.05, **P < 0.01, ***P < 0.001.

nanoparticles system on E0771 cells was further detected by apoptosis assays kit. E0771 cells treated with nano-drugs were double stained with annexin V-FITC and propidium iodide (PI). As shown in Fig. 3C and D and Figs. S14–15, all the materials used shared no obvious cytotoxicity on E0771 cells and normal liver cells, indicating biosafety of the virus-mimicking nanoparticles. Total apoptosis rate of iaCRP/pTRAIL group was 50.77 %, which was much higher than that of bCRP/pTRAIL (13.1 %) and aCRP/pTRAIL (29.4 %). The results indicated that the active targeting and uptake of tumor cells mediated by iRGD-apoA-I led to increased apoptosis. In the unresponsive iaCPP/pTRAIL group, total apoptosis rate of tumor cells was 19.5 %, significantly lower than that in iaCRP/pTRAIL group. The results indicated that rapid release of pTRAIL mediated by ROS-responsive CRP polymers played a vital role in the induction of apoptosis. The cytotoxicity of the virus-mimicking nanoparticles was further estimated in E0771 cells, ROS-eliminated E0771 cells, Chang Liver cells and ROS-treated Chang Liver cells to validate site-specific antitumor efficacy (Fig. S16). iaCRP/pTRAIL demonstrated remarkable cell viability reduction of ~70 %, while only 16 % cell viability reduction was observed in ROS-eliminated E0771 cells. In Chang Liver cells, cell viability reduction is less than 10 %, but decreased to 42 % in H_2O_2 pre-treated group. The results indicated that the transfection efficacy is controlled by intracellular ROS concentration, which could guarantee high TRAIL expression in tumor cells for advanced therapeutic benefits, and avoid cytotoxicity against normal cells. Collectively, the above results confirmed that iaCRP/pTRAIL provided an advanced anti-tumor efficacy, laying a foundation for subsequent *in vivo* therapeutic effect investigation. Based on the high transfection of pTRAIL and efficient apoptosis induction of virus-mimicking nanoparticles, TRAIL-specific bystander effect was further evaluated. When the tumor cells were transfected by the virus-mimicking nanoparticles, highly-expressed TRAIL protein would be secreted to intercellular substance. Since tumor cells are densely distributed inside the tumor tissue, the secreted TRAIL protein could not only bind to death receptors on the transfected tumor cells themselves, but also bind to death receptors neighboring tumor cells to induce extensive apoptosis. As shown in Fig. 3E, E0771 breast cancer cells were treated with virus-mimicking nanoparticles and further cultured for 48 h. The supernatant of cell culture was collected by centrifugation to

incubate with normal E0771 cells, followed by apoptosis-inducing effect detection annexin V-FITC/PI cell apoptosis assay at 24 h. The bystander effect of iaCRP/pTRAIL (s) group gave the highest apoptosis of ~40 %, compared with aCRP/pTRAIL (s), bCRP/pTRAIL (s), and iaCPP/pTRAIL (s) groups (Fig. 3F and G). The results could be mainly ascribed to advanced TRAIL expression of iaCRP/pTRAIL from tumor cell targeting internalization and responsive pTRAIL release. The bystander effect was supposed to enhance the anti-tumor efficacy of TRAIL-specific therapy by eliminating neighboring tumor cells and metastasis.

3.6. In vivo imaging and biodistribution

The biosafety of the nanoparticles was investigated before *in vivo* experiments. iaCRP/pTRAIL nanoparticles shared negligible hemolysis (Fig. S17) due to the biomimetic surface decoration of iRGD-apoA-I. After administration of nanoparticles, no obvious heart, liver, or renal dysfunction was detected (Fig. S18), and no pathological damage in the main organs was observed (Fig. S19). To evaluate the *in vivo* tumor targeting effect, iaCRP/Cy5-pTRAIL, aCRP/Cy5-pTRAIL, and bCRP/Cy5-pTRAIL were prepared using Cy5-pTRAIL and injected intravenously into mice. The biodistribution of nanoparticles in mice was visualized by noninvasive near-infrared optical imaging within 24 h after injection. As shown in Fig. 4A, iaCRP/Cy5-pTRAIL nanoparticles could reach the tumor site at 4 h post injection, while in groups of bCRP/Cy5-pTRAIL and aCRP/Cy5-pTRAIL, the fluorescence signal at tumor site could be detected at 8 h post injection. The fluorescence intensity of iaCRP/Cy5-pTRAIL nanoparticles at the tumor site kept increasing within 24 h, which could benefit from biostability of the virus-mimicking nanoparticles design in circulation. At each time interval, fluorescence intensity at tumor site of iaCRP/Cy5-pTRAIL group was higher than that of bCRP/Cy5-pTRAIL and aCRP/Cy5-pTRAIL nanoparticles. The results indicated that iRGD-apoA-I significantly improved the tumor targeting of iaCRP/Cy5-pTRAIL through NRP-1 receptor in tumor tissue. The main organs including heart, liver, spleen, lung, kidney, and tumor tissues of each group were collected for *ex vivo* imaging at 24 h post injection. The fluorescence intensity of iaCRP/Cy5-pTRAIL in tumor tissue was about 2-fold higher than that of bCRP/pTRAIL group, and 1.7-fold higher than that of aCRP/pTRAIL group (Fig. 4B and C). Moreover, liver fluorescence of iaCRP/Cy5-pTRAIL is notably lower than that of bCRP/Cy5-pTRAIL. The results further confirmed iRGD-apoA-I mediated tumor-selective accumulation from virus-mimicking nanoparticles, which was beneficial for enhanced anti-tumor effect and attenuated potential side effects. The tumor tissues of each group were thereafter sliced to investigate intratumoral distribution of the nanoparticles via CLSM. As illustrated in Fig. 4D, iaCRP/Cy5-pTRAIL shared the strongest fluorescence signal, along with homogeneous distribution, indicating effective tumor penetration of iaCRP/Cy5-pTRAIL nanoparticles.

3.7. In vivo TRAIL-specific bystander effect research

TRAIL-specific bystander effect was also evaluated in pulmonary metastasis model *in vivo*. As shown in Fig. 4E, TRAIL homozygous knockout C57BL/6 mice were employed to establish a lung metastasis model of breast cancer by intravenous injection of E0771 cells. Different nanoparticles were used to transfect E0771 cells, and the supernatant of

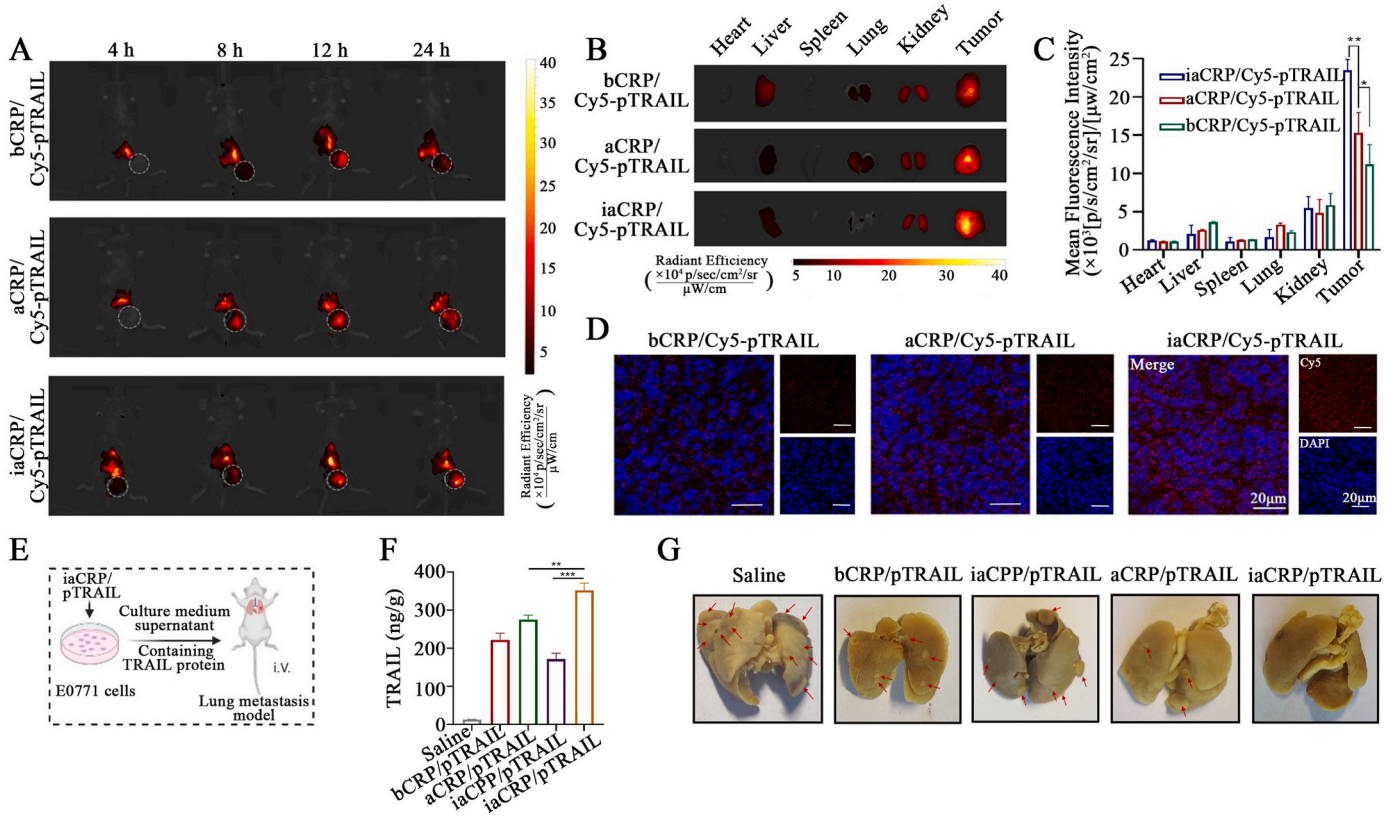

Fig. 4. Biodistribution of virus-mimicking nanoparticles and TRAIL-specific bystander effect. (A) *In vivo* imaging of E0771 tumor-bearing mice after injection of iaCRP/Cy5-pTRAIL, aCRP/Cy5-pTRAIL, and bCRP/Cy5-pTRAIL at 4, 8,12, and 24 h. (B) Fluorescence imaging of major organs and tumors at 24 h post-injection. (C) Quantification of mean fluorescence intensity in main organs and tumors at 24 h post-injection. (D) CLSM images of E0771 tumor sections at 24 h after injection of nano-systems. (E) Schematic diagram of *in vivo* bystander effect of TRAIL therapy. Virus-mimicking nanoparticles were employed to transfect E0771 cells, and supernatant of culture medium was collected for further intravenous administration to lung metastasis bearing mice. (F) Determination of TRAIL protein concentration in the lungs of mice with tumor metastasis after administration by ELISA method. (G) Representative photos of the lungs collected from the *in vivo* bystander effect research groups. Results were presented as mean ± S.D. (n = 3), *P < 0.05, **P < 0.01, ***P < 0.001.

culture medium in each group was collected for further intravenous administration to lung metastasis bearing mice. The mice were administrated once a day for 5 times, and lungs of each group were collected at 1 h after the last administration. TRAIL concentration in the lungs was detected by enzyme linked immunosorbent assay (ELISA) kit (Fig. 4F and G). Lungs of iaCRP/pTRAIL group gave the highest TRAIL protein concentration, and pulmonary metastatic nodules could hardly be observed. The results indicated that iaCRP/pTRAIL treated tumor cells could generate an effective dose of TRAIL protein, which could maintain biological activity in circulation for distant metastasis elimination. The *in vivo* transfection of tumor cells via virus-mimicking nanoparticles was also supposed to give similar anti-metastasis effect.

3.8. *In vivo* therapeutic efficacy against breast cancer

In vivo anti-tumor efficacy of the virus-mimicking nanoparticles was evaluated in an orthotopic breast cancer model. When the tumor volume reached 200 mm^3, the mice were treated with saline, aCRP/pTRAIL, bCRP/pTRAIL, iaCPP/pTRAIL, and iaCRP/pTRAIL every three days for 6 times. Tumor volume variations were shown in Fig. 5A. Compared

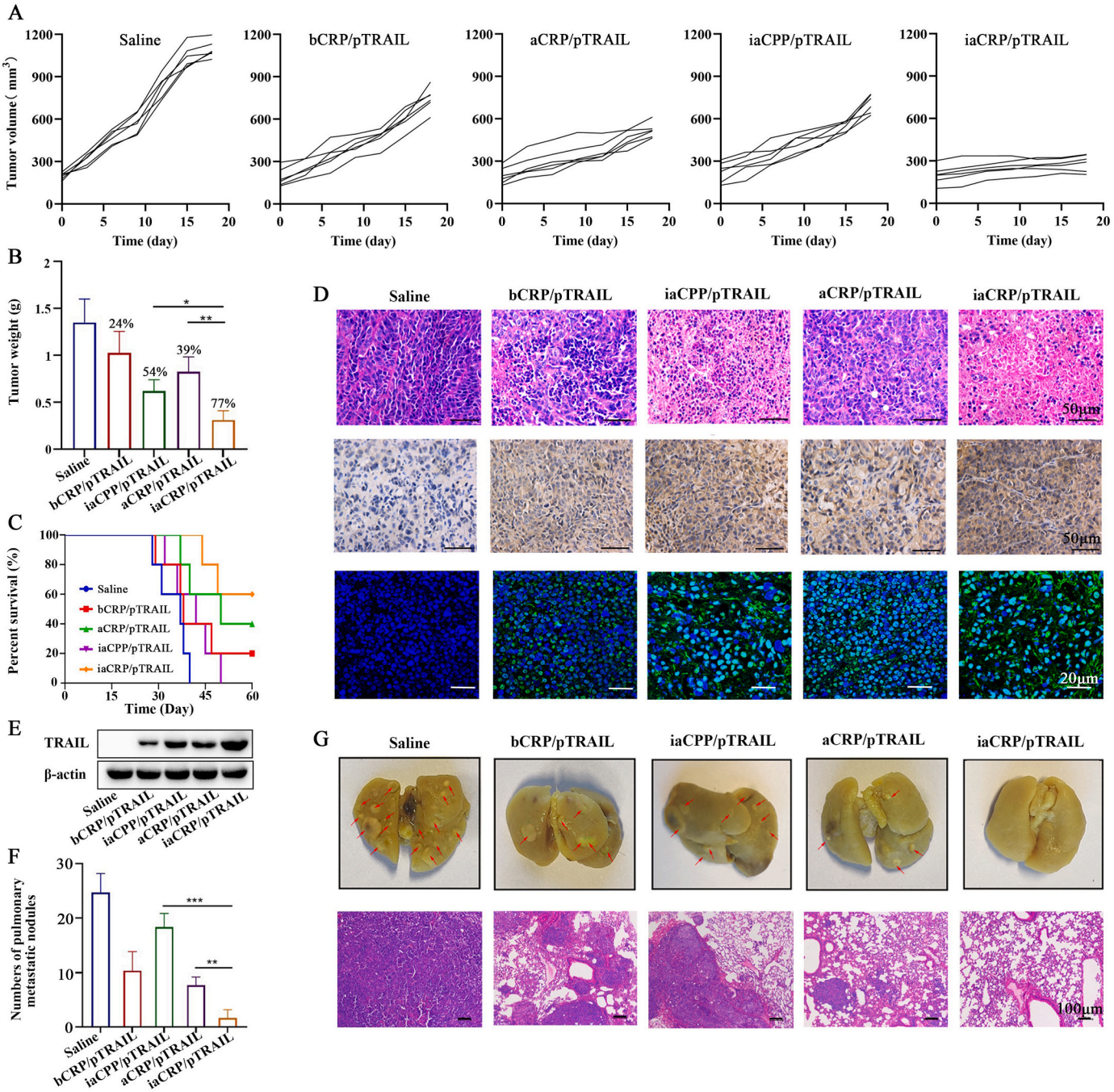

Fig. 5. *In vivo* antitumor efficiency of iaCRP/pTRAIL against breast cancer. (A) *In vivo* tumor volume change curves of the study groups. (B) Tumor weight and tumor inhibition rate of the study groups. (C) Survival rates of the studied animals. (D) Histological analysis of tumor sections stained with H&E and TUNEL staining of E0771 tumor tissues after treatments, and TRAIL expression in tumor tissues via immunohistochemical staining. (E) Western-blotting analysis of TRAIL expression in tumors treated with different preparations. (F) Pulmonary metastatic nodules numbers of E0771 tumor xenograft C57 mice after treatments. (G) Representative images of H&E staining of lungs collected from different groups. Results were presented as mean ± S.D. (n = 3), *P < 0.05, **P < 0.01, ***P < 0.001.

with saline group, all treatment groups performed different degrees of tumor growth inhibition, where iaCRP/pTRAIL yielded the highest tumor suppression. bCRP/pTRAIL and iaCPP/pTRAIL groups displayed similar insufficient anti-tumor effects, which were mainly ascribed to non-targeting distribution and tardy pTRAIL release, respectively. The tumor inhibition efficacy of aCRP/pTRAIL was attenuated due to lack of iRGD mediated tumor-selective penetration. No abnormal body weight variation was observed during the treatment (Fig. S20). Mice were sacrificed at day 18, and the tumors were excised and weighed (Fig. 5B). The tumor weight analysis further validated that iaCRP/pTRAIL was the most effective in tumor growth inhibition. The survival rate of mice in each group was investigated at the end of the study. After 60 days, the survival rates of bCRP/pTRAIL, aCRP/pTRAIL, and iaCRP/pTRAIL group were 20 %, 40 %, and 60 %, respectively, while all mice of saline group died within 40 days (Fig. 5C). The results suggested dramatic improvement of mice survival after iaCRP/pTRAIL treatment, benefiting from the efficient tumor targeting and swift pTRAIL release. In the pathological examination of the tumors (Fig. 5D), considerably enhanced necrosis in terms of dissolved and broken cancer cells was observed in iaCRP/pTRAIL group when compared with the control groups. Terminal-deoxynucleoitidyl transferase mediated nick end labeling (TUNEL) staining was further employed to evaluate cell apoptosis in tumor tissues. Tumors of iaCRP/pTRAIL group shared significantly elevated level of TUNEL biomarkers, suggesting prominent tumor apoptosis. TRAIL expression levels were synchronously estimated via immunohistochemical staining and western blot (Fig. 5D and E). TRAIL levels in each group were in consistence with TUNEL signals. The results indicated that the anti-tumor efficacy was mainly derived from TRAIL high-expression, and the tumor-targeting delivery and swift pTRAIL dissociation were of great importance for effective transfection.

At the end of the survival investigation, the intact lungs of each group were collected for evaluation on anti-metastasis activity from bystander effect. As shown in Fig. 5F and G, the nodular metastasis was stained by Bouin's solution, and the number of nodules was counted. iaCRP/pTRAIL group performed nearly no metastasis nodule, indicating an efficient metastasis blocking via TRAIL-specific bystander effect. The lungs were further subjected to H&E staining where normal lung tissue revealed reticular structure, and metastatic lesions of dense cell masses. A large area of dense tumor tissue could be observed in saline group, and the percentage of tumor tissue gave slight shrinkage in bCRP/pTRAIL and iaCPP/pTRAIL groups. A small amount of tumor tissue could be observed in some areas of lung tissue in aCRP/pTRAIL group, while no apparent tumor tissue was found in iaCRP/pTRAIL group. Therefore, virus-mimicking nanoparticles mediated efficient pTRAIL transfection could contributed enhanced bystander effect for elimination of distant metastasis.

4. Conclusions

In summary, a virus-mimicking nanoparticle was developed for efficient pTRAIL delivery and transfection in site-specific apoptosis and bystander effects. The ROS-respective polymer CRP provided both high gene compression and triggerable swift gene liberation, which guaranteed the high transfection after site-specific cell internalization. Moreover, a tailor-made capsid of iRGD-apoA-I was constructed to protect pTRAIL compression and mediated tumor targeting and penetrating delivery. The "gene core-protein shell" virus-mimicking strategy could induce high TRAIL expression both *in vitro* and *in vivo*, which could mobilize enhanced bystander effect for elimination of primary and metastasis tumor. Collectively, the virus-mimicking nanoparticle strategy provided a promising solution for efficient and safe gene oncotherapy.

CRediT authorship contribution statement

Ruirong Wu: Writing – original draft, Visualization, Methodology, Investigation, Funding acquisition, Formal analysis, Data curation. **Xiufeng Wu:** Writing – original draft, Visualization, Methodology, Investigation, Funding acquisition, Formal analysis, Data curation, Conceptualization. **Lan Zhang:** Software, Methodology, Investigation, Data curation. **Feng Zhang:** Methodology, Investigation. **Yang Ding:** Writing – review & editing, Supervision, Project administration, Conceptualization. **Yong Mao:** Writing – review & editing, Supervision, Resources, Funding acquisition, Conceptualization. **Jiang Ni:** Writing – review & editing, Writing – original draft, Validation, Supervision, Project administration, Funding acquisition, Formal analysis, Conceptualization.

Declaration of competing interest

The authors declare that they have no known competing financial interests or personal relationships that could have appeared to influence the work reported in this paper.

Acknowledgements

The authors gratefully acknowledge the Natural Science Foundation of Jiangsu Province (BK20240299), Wuxi City Social Development Science and Technology Demonstration Project (N20201005), Wuxi Municipal Health Commission Youth Research Project (Q202201, Q202230), and the Top Talent Support Program for young and middle-aged people of Wuxi Health Committee (BJ2023063). We thank the Cellular and Molecular Biology Center of China Pharmaceutical University for assistance with CLSM.

Appendix A. Supplementary data

Supplementary data to this article can be found online at https://doi.org/10.1016/j.mtbio.2025.101633.

Data availability

Data will be made available on request.

References

[1] D. Mai, C.H. June, N.C. Sheppard, In vivo gene immunotherapy for cancer, Sci. Transl. Med. 14 (670) (2022) eabo3603.
[2] K.A. High, M.G. Roncarolo, Gene therapy, N. Engl. J. Med. 381 (5) (2019) 455–464.
[3] H.Z. Yang, Y. Guo, L. Pu, X.Q. Yu, J. Zhang, Fluorescent self-reporting lipid nanoparticles for nitric oxide/gene Co-delivery and combination therapy, Mol. Pharm. 20 (2) (2023) 1404–1414.
[4] J.T. Bulcha, Y. Wang, H. Ma, P.W.L. Tai, G. Gao, Viral vector platforms within the gene therapy landscape, Signal Transduct. Targeted Ther. 6 (1) (2021) 53.
[5] A. Raguram, S. Banskota, D.R. Liu, Therapeutic in vivo delivery of gene editing agents, Cell 185 (15) (2022) 2806–2827.
[6] D.W. Brown, P. Wee, P. Bhandari, A. Bukhari, L. Grin, H. Vega, M. Hejazi, D. Sosnowski, J. Ablack, E.K. Clancy, D. Pink, J. Kumar, M.P. Solis Ares, S. Lamb, R. Quevedo, B. Rawal, F. Elian, N. Rana, L. Morales, N. Govindasamy, B. Todd, A. Delmage, S. Gupta, N. McMullen, D. MacKenzie, P.H. Beatty, H. Garcia, M. Parmar, J. Gyoba, C. McAllister, M. Scholz, R. Duncan, A. Raturi, J.D. Lewis, Safe and effective in vivo delivery of DNA and RNA using proteolipid vehicles, Cell 187 (19) (2024) 5357–5375, e24.
[7] S. Banskota, A. Raguram, S. Suh, S.W. Du, J.R. Davis, E.H. Choi, X. Wang, S. C. Nielsen, G.A. Newby, P.B. Randolph, M.J. Osborn, K. Musunuru, K. Palczewski, D.R. Liu, Engineered virus-like particles for efficient in vivo delivery of therapeutic proteins, Cell 185 (2) (2022) 250–265, e16.
[8] Y.L. Chen, C.J. Bao, J.L. Duan, Y. Xie, W.L. Lu, Overcoming biological barriers by virus-like drug particles for drug delivery, Adv. Drug Deliv. Rev. 203 (2023) 115134.
[9] M. Huang, X. Pan, X. Wang, Q. Ren, B. Tong, X. Dong, G. Ge, L. Lu, S. Jiang, J. Chen, Lymphocyte integrins mediate entry and dysregulation of T cells by SARS-CoV-2, Signal Transduct. Targeted Ther. 8 (1) (2023) 84.
[10] Y. Pan, Q. Xue, Y. Yang, T. Shi, H. Wang, X. Song, Y. Luo, W. Liu, S. Ren, Y. Cai, Y. Nie, Z. Song, B. Liu, J.P. Li, J. Wei, Glycoengineering-based anti-PD-1-iRGD peptide conjugate boosts antitumor efficacy through T cell engagement, Cell Rep. Med. 5 (6) (2024) 101590.

[11] L. Lu, X. Zhao, T. Fu, K. Li, Y. He, Z. Luo, L. Dai, R. Zeng, K. Cai, An iRGD-conjugated prodrug micelle with blood-brain-barrier penetrability for anti-glioma therapy, Biomaterials 230 (2020) 119666.
[12] S. Busatto, S.A. Walker, W. Grayson, A. Pham, M. Tian, N. Nesto, J. Barklund, J. Wolfram, Lipoprotein-based drug delivery, Adv. Drug Deliv. Rev. 159 (2020) 377–390.
[13] D. Witzigmann, J.A. Kulkarni, J. Leung, S. Chen, P.R. Cullis, R. van der Meel, Lipid nanoparticle technology for therapeutic gene regulation in the liver, Adv. Drug Deliv. Rev. 159 (2020) 344–363.
[14] S. Peng, F. Xiao, M. Chen, H. Gao, Tumor-microenvironment-responsive nanomedicine for enhanced cancer immunotherapy, Adv. Sci. 9 (1) (2022) e2103836.
[15] C. Mao, S. Yeh, J. Fu, M. Porosnicu, A. Thomas, G.L. Kucera, K.I. Votanopoulos, S. Tian, X. Ming, Delivery of an ectonucleotidase inhibitor with ROS-responsive nanoparticles overcomes adenosine-mediated cancer immunosuppression, Sci. Transl. Med. 14 (648) (2022) eabh1261.
[16] X. Wang, S. Yin, M. Li, J. Rao, D. Wan, Y. Qiu, Q. Yu, X. Chen, Z. Lu, Y. Long, Z. Zhang, Q. He, Autophagy inhibition changes the disposition of non-viral gene carriers during blood-brain barrier penetration and enhances TRAIL-induced apoptosis in brain metastatic tumor, J. Contr. Release 321 (2020) 497–508.
[17] H. Zhang, S. Dong, Z. Li, X. Feng, W. Xu, C.M.S. Tulinao, Y. Jiang, J. Ding, Biointerface engineering nanoplatforms for cancer-targeted drug delivery, Asian J. Pharm. Sci. 15 (4) (2020) 397–415.
[18] X. Li, X. Sun, B. Wang, Y. Li, J. Tong, Oncolytic virus-based hepatocellular carcinoma treatment: current status, intravenous delivery strategies, and emerging combination therapeutic solutions, Asian J. Pharm. Sci. 18 (1) (2023) 100771.
[19] M. Habibizadeh, S. Lotfollahzadeh, P. Mahdavi, S. Mohammadi, O. Tavallaei, Nanoparticle-mediated gene delivery of TRAIL to resistant cancer cells: a review, Heliyon 10 (16) (2024) e36057.
[20] R. Wang, X. Gu, J. Zhou, L. Shen, L. Yin, P. Hua, Y. Ding, Green design "bioinspired disassembly-reassembly strategy" applied for improved tumor-targeted anticancer drug delivery, J. Contr. Release 235 (2016) 134–146.
[21] E.C. Cheung, K.H. Vousden, The role of ROS in tumour development and progression, Nat. Rev. Cancer 22 (5) (2022) 280–297.